



ON THE NON-LINEAR INFLUENCE OF THE EDGE GEOMETRY ON VORTEX SHEDDING IN HELMHOLTZ RESONATORS

Kilian Förner^{1†}, Muttalip Aşkın Temiz², Wolfgang Polifke¹, Ines Lopez Arteaga², and Avraham Hirschberg³

¹*Professur für Thermofluidodynamik, Technische Universität München, Germany*

[†] *e-mail: foerner@afd.mw.tum.de*

²*Eindhoven University of Technology, Dept. of Mechanical Engineering, Eindhoven, The Netherlands.*

³*Eindhoven University of Technology, Dept. of Applied Physics, Eindhoven, The Netherlands.*

This study investigates the effect of edge profile of a Helmholtz resonator neck in non-linear regime by means of experiments and large eddy simulations. The dissipation mechanisms in a Helmholtz resonator differ significantly, depending on the sound pressure level. At low levels, i. e., in the linear regime, thermo-viscous effects are responsible for the dissipation of the acoustic energy since the oscillating flow follows the neck geometry. However, increasing the sound pressure level results in flow separation at the edges. At these points, vortices form which convert acoustic perturbation energy to the hydrodynamic mode. This is a strong non-linear effect increasing the dissipation considerably. To observe this effect, experiments and numerical simulations are carried out for combinations of various backing volumes, sound pressure levels, and neck profiles. The neck profiles are selected as 45°-chamfers due to manufacturing concerns. Hereby, a strong dependence on the edge shape is observed in both experiments and numerical simulations. The presence of the chamfer reduces the vortex shedding in comparison to the sharp edge significantly, which leads to a lower acoustic resistance.

1. Introduction

Helmholtz resonators are passive sound absorbers having a wide range of application areas from ancient Greek theaters [1] to aerospace industry [2]. These resonators are named after the first scientist to analyze them theoretically: Hermann von Helmholtz [3].

A Helmholtz resonator is a combination of an air *backing volume* and an opening, which is referred to as the *neck* of the resonator. When excited by a pressure perturbation, the air volume acts as a spring due to its compressibility and causes oscillation of the air in the neck. This spring-mass model is introduced by Rayleigh [4] simplifying Helmholtz's pioneer work. Later, Ingard and Labate [5] observed that there are two main dissipation mechanisms in the Helmholtz resonators. The first is due to thermo-viscous boundary layers, which is linear; and the other one is due to vortex shedding, which is non-linear. This non-linear dissipation effect is addressed by Ingard and Ising [6]. They considered the neck separately, performed pressure as well as particle velocity measurements, and observed that this non-linear mechanism causes a decrease in the reactance of the oscillating air within the neck.

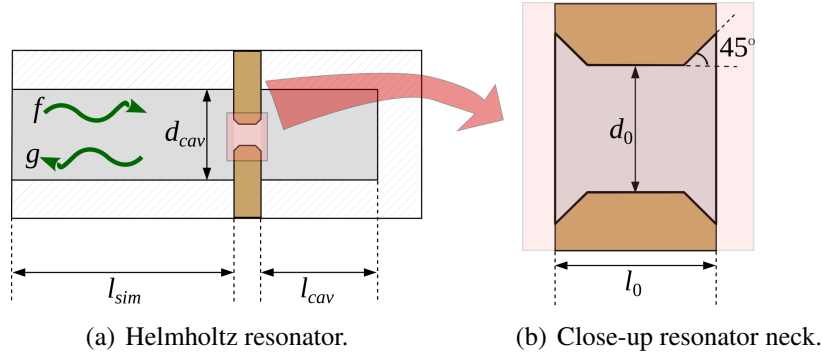


Figure 1. Sketch of the Helmholtz resonator geometry.

In 1979, Hersh *et al.* [1] derived non-linear differential equations to model the non-linear response of the Helmholtz resonators. Yet none of the studies mentioned so far focuses on the effect of the edge profile of the neck on the non-linearity of the resonator. In similar configurations, a huge impact of the edge geometry was observed, see, e. g., the study for a resonance tube by Disselhorst and van Wijngaarden [7].

In this study, three different neck samples are used. One of these samples has the sharp and other two have the 45°-chamfered edge profile in combination with different chamfer lengths. The purpose of the study is to understand the effect of edge profile of the neck on the non-linear response of the Helmholtz resonator. To achieve this purpose, large eddy simulations (LES) and impedance tube measurements are carried out. The geometry of the Helmholtz resonator domain is sketched in Fig. 1.

2. Modeling of Helmholtz Resonators

The dynamic behavior of the Helmholtz resonator is commonly described in frequency domain with its *surface impedance* Z_s . The impedance is defined as the ratio of the Fourier transforms of the fluctuating pressure \hat{p}' to the fluctuating velocity \hat{u}' , i. e., $Z_s(\omega) = \hat{p}'(\omega)/\hat{u}'(\omega)$. Thus, the impedance Z_s can be seen as transfer function from u' to p' . The real part of the impedance is referred to as the so-called *resistance* and the imaginary as *reactance*. Such a description in frequency domain is actually only valid for linear transfer functions. The non-linear dynamic response of resonators is commonly given by describing functions. That means that the impedance is defined depending on the amplitude. This approach neglects higher harmonics. Nevertheless, it reflects the major dynamics well. As mentioned above, the behavior of the resonator is often described as mass-spring-damper system and reads as

$$(1) \quad Z_s(\omega) = R_l + R_{nl} + i(m\omega - K/\omega).$$

Here, the term m accounts for the mass in the neck taking part in the oscillation and K for the compressibility of the backing volume. The variable R_l denotes the linear resistance reflecting for the thermo-viscous losses due to friction at the walls of the neck. If the amplitudes are large enough, the flow separates at the edges transforming additional energy to the hydrodynamic mode from the acoustic mode, which is irrotational by definition. This is a non-linear mechanism depending on the current amplitude and is captured by the term R_{nl} . All terms in Eq. (1) are determined by analytical models but they also contain some empirical correlation values. According to Keller and Zauner [8] and Garrison *et al.* [9], they are approximately given as

$$(2) \quad m = (1 + s) l_e \bar{\rho}, \quad K = \frac{A \bar{\rho} c^2}{V}, \quad R_l = s \bar{\rho} (l_0 + l_s) \omega, \quad \text{and} \quad R_{nl} = \epsilon_{nl} s \bar{\rho} d_0 \omega,$$

where the mean pressure, density, and speed of sound are denoted by \bar{p} , $\bar{\rho}$, and c , respectively. The geometry is described by the backing volume V as well as by the neck area A , and length l_0 . The

boundary layer effects are included in the parameter s^1 . The effective mass oscillating around the neck is determined by adding a correction to the neck length. Similarly for the viscous losses, l_0 is extended by l_s . The non-linear losses are captured by the non-linear correlation factor ϵ_{nl} . The angular eigenfrequency of the resonator is given as the ratio of m to K , thus $\omega_{eig} = c \sqrt{A/(V(1+s)l_e)}$. In the following, the impedance Z_s is normalized by the free impedance $\bar{\rho}c$, i. e., $Z = Z_s/(\bar{\rho}c)$.

In the resonance tube located in front of the resonator, the acoustic field can be described by the Riemann invariants defined as $f = 1/2(p' / (\bar{\rho}c) + u')$ and $g = 1/2(p' / (\bar{\rho}c) - u')$ and depicted in Fig 1. In terms of these quantities, the impact of the Helmholtz resonator is determined by the reflection coefficient $R = g/f$. The relation between this coefficient R and the normalized impedance Z is given by $Z = (1 + R)/(1 - R)$.

3. Setup

Several test cases are investigated both numerically and experimentally. These cases consist of combinations of three different neck profiles and two different backing volume lengths l_{cav} in a resonance tube with diameter d_{cav} . The considered necks have the same length l_0 and diameter d_0 but differ in their edge profiles. One of the necks has a sharp edge ($l_c = 0$) where the other two have 45°-chamfers with different sizes l_c . The geometrical specifications are given in Tab. 1. The reflection behavior of these test cases is studied for various SPLs, in particular for 89.3, 115.6, and 119.7 dB.

Table 1. Geometric properties (in mm).

Considered chamfer lengths			Volume lengths		Common parts		
l_c	l_c	l_c	l_{cav}	l_{cav}	l_0	d_0	d_{cav}
0	0.35	1.0	10	20	4.0	4.2	50

3.1 Experimental Setup

The experiments have been carried out with an impedance tube in an semi-anechoic chamber. The tube has six BSWA MPA416 microphones with the average sensitivity of 50.45 mV/Pa. They are equally distributed along the 1-m long tube and the distances between two successive microphones are 175 mm. The microphones are relatively calibrated to carry out reflection coefficient measurements from 100 Hz to 700 Hz. The inner diameter of the tube, d_{cav} , is 50 mm.

The data acquisition and signal processing is done by a combination of NI PCIe-6361 X-Series DAQ card and LabView[®]. One analogue output channel for the loudspeaker and six analogue input channels for microphones are used. The sampling rate for generated signal is 20 kHz while it is 10 kHz for recording. The closest microphone to the tube termination is selected as the reference input. The LabView[®] script regulates the excitation amplitude of the loudspeaker for each frequency step. Doing so, it is possible to have the same – or very close – SPLs throughout the entire frequency span. It is important to note here that this reference microphone is placed 49.7 mm away from the tube termination. Accordingly, the SPLs are calculated at this position. The reference position would ideally be located at the resonator mouth, but due to physical constraints, placing a microphone at that position was not possible in this setup.

Some precautions are taken to minimize the measurements errors. First, the recorded data from the microphones are processed using a lock-in method instead of using FFT. Secondly, the visco-thermal effects in the tube are included [10] and implemented in the wave decomposition [11]. Finally, instead

¹ $s = (1 + (\kappa - 1)/\sqrt{Pr})\sqrt{2\nu/\omega}/d_0$, where the variables Pr , κ , and ν denote the Prandtl number, the heat capacity ratio, and the kinematic viscosity, respectively.

of assuming a value for the speed of sound, it is treated as an extra unknown in the over-determined set of equations [12]. With all these specifications and precautions, the deviation from the theoretical closed-end reflection coefficient value is less than 0.5 % in the frequency of interest.

3.2 Numerical Setup

The compressible Navier-Stokes equations with k-equation eddy-viscosity subgrid-scale model are solved in 3D using the Pimple algorithm of OpenFOAM [13]. The tolerance for stop criterion for outer iteration loops accounting for compressible pressure-velocity coupling are set low – i. e., accurate – enough to resolve the acoustic field in details. Here, a threshold for the pressure residual of 10^{-5} was applied. The time step size Δt is adjusted such that the acoustic CFL number $c \Delta t / \Delta x$ is clearly below unity in the main parts. Only close to the walls, this number can be slightly larger, but the acoustic behavior is still resolved accurately in those regions due to implicit time integration.

The geometrical dimensions of the neck configurations and of the backing volumes are set in analogy to the experimental setup properties summarized in Tab. 1. At the corresponding boundaries, the no-slip condition is utilized. The slip condition is used at the cylindrical wall of the impedance tube which does not belong to the resonator itself. For each geometry investigated, a structured o-grid mesh with at least 0.8 million cells is set up. Hereby especially, the boundary layer, whose thickness can a priori be estimated by the Stokes length $\delta_s = 2\pi\sqrt{2\nu/\omega}$, must be resolved well for the frequencies of interest. In the linear regime, grid independence studies and validation have proved the appropriateness of such a setting, see [14].

At the distance $l_{sim} = 10$ cm, the inlet patch is located, where the Navier-Stokes characteristics boundary condition (NSCBC), c. f. [15], is applied. This boundary condition ensures a low acoustic reflection of the outgoing g wave. Simultaneously, an input signal can be imposed for the incoming f wave. At this inlet plane, the fluctuating pressure p' and velocity u' are measured. From these quantities, the time series of the Riemann invariants f and g can be computed directly. For that purpose, the distance l_{sim} is chosen large enough such that non-acoustic disturbances as the vortices present in the vicinity of the neck do not influence the measurement.

The reflection coefficient is estimated from the measured input f and output g time series. First, these time series are shifted with respect to each other to account for the time it takes to travel from the reference plane to the resonator and back. Then for the identification, two approaches are applied depending of the present regime. In the linear regime corresponding to a low SPL as 89.3 dB, linear system identification techniques are used. Here, the domain is excited with a well-designed broadband signal. From the response, a second order Output-Error model is estimated, valid for the whole frequency range of interest [14]. In the non-linear regime with higher amplitudes, harmonic simulations are performed with several angular frequencies ω_m . For the determination of the numerical $R_{num}(\omega_m) = \text{fft}(g)(\omega_m) / \text{fft}(f)(\omega_m)$, the signals are additionally truncated to get rid of the transient starting behavior and to have a signal length of a multiple of the period $1/(2\pi\omega_m)$. The amplitude of the input signal f is calculated according to the the experimental data.

4. Results

Gain and phase of the reflection coefficient are presented for the SPLs investigated for all cases with $l_{cav} = 20$ mm in Fig. 2. The reflection coefficient is transformed to the normalized surface impedance Z , using the relation $Z = (1 + R)/(1 - R)$ and plotted in Fig. 3. Due to lack of space, only the results for the backing volume with 20 mm length are shown in the present paper. The following discussions and findings are equally supported by the other cases with 10 mm backing volume length.

For all geometries, experiment and simulation agree very well in the linear regime. The evaluation of the 89.3 dB simulations confirms that the flow does not separate at the edges. That means that the Stokes boundary layer is resolved sufficiently in the simulations to capture the thermo-viscous dissipation taking place in that region. In the non-linear regime, the agreement is only of qualitative, but

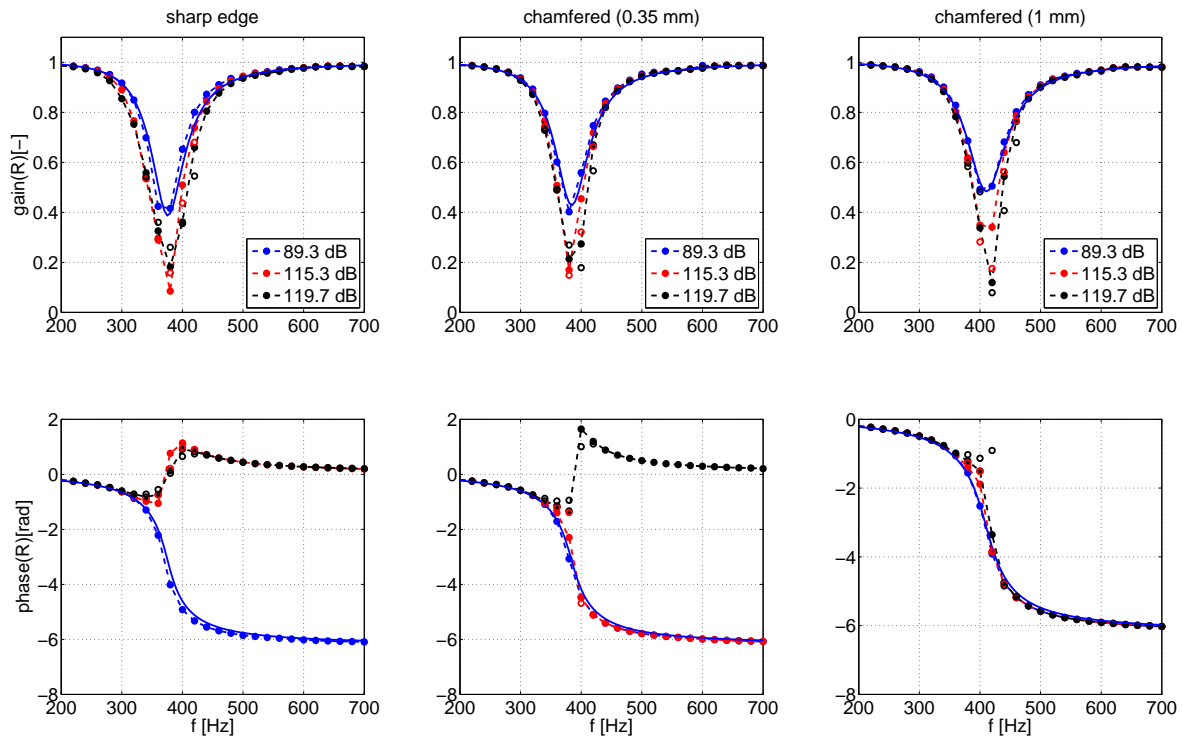


Figure 2. Reflection coefficient in gain and phase representation for all configurations with $l_{cav} = 20$ mm. "—●—": measurement results; "—": linear SI results; and "○": harmonic simulation results. The colors correspond to different SPLs as indicated by the legends in the subfigures.

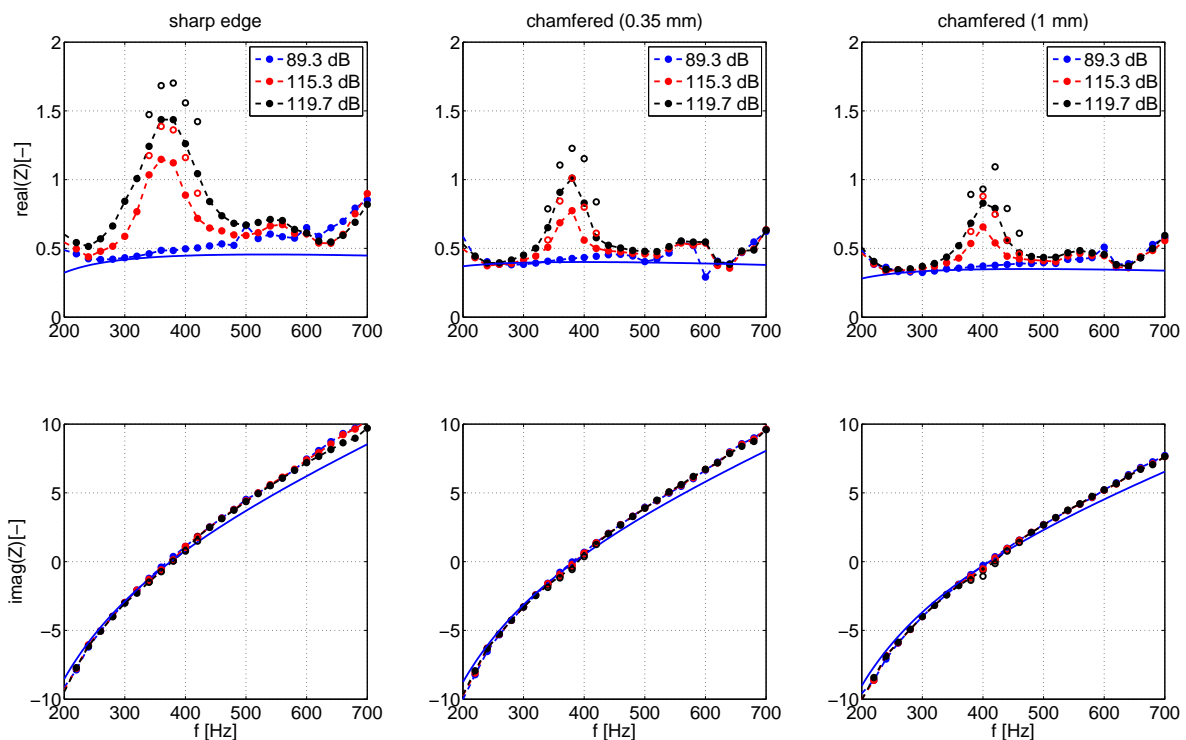


Figure 3. Normalized impedance determined in resistance and reactance representation for all configurations with $l_{cav} = 20$ mm. "—●—": measurement results; "—": linear SI results; and "○": harmonic simulation results. The colors correspond to different SPLs as indicated by the legends in the subfigures.

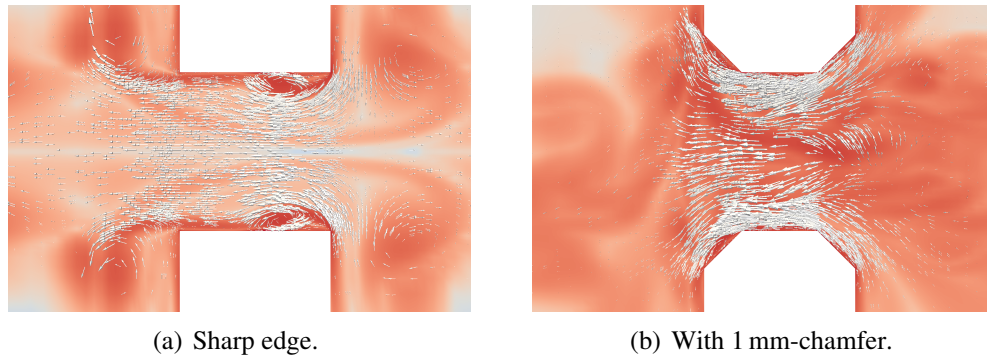


Figure 4. Snapshots of the velocity field (white arrows) in the neck during the outflow with 119.7 dB.

not of quantitative nature. The reactance $\Im(Z)$ curves still match for all cases and amplitudes in that regime. But, the non-linear resistance is systematically over-predicted by the numerical simulations for all cases. The reason for this over-prediction is topic of ongoing research. The grid dependency as well as the influence of the sub-grid scale modeling have to be studied in more detail. Another reason might be that the edges are perfectly sharp in the simulation, whereas they are not in reality. Nevertheless, the simulations provide a detailed view on the flow present in the resonator. The following statements are confirmed by both experiment and simulation in the same manner.

First, the influence of the edge geometry on the eigenfrequency is discussed. This is a linear effect and, thus, independent on the current SPL. Only for very high amplitudes beyond the SPL considered in this study, the eigenfrequency is nominally influenced by the amplitude, see for instance [1]. The eigenfrequency can be detected by the minimal gain of the reflection coefficient. The corresponding phase is either $-\pi$ in the non-over-damped case or 0 in the over-damped case. Moreover, the reactance $\Im(Z)$ vanishes at the eigenfrequency. With these criteria, a shift of the eigenfrequency towards higher frequencies with increasing the chamfer size can be observed. In the specific case of 20 mm cavity length, the eigenfrequency rises from around 375 Hz without a chamfer, to approximately 385 Hz and 410 Hz with the 0.35 mm and 1 mm-chamfer, respectively. This shift can be explained by a reduction of the effective length with increasing the chamfer length. For the three cases, the resulting effective length are 7.19 mm, 6.82 mm, and 6.02 mm, respectively. The detected effective length of the unchamfered case go in line with the correlation by Ingard [16]. He suggested for large aspect ratios ($d_0/\sqrt[3]{V} \ll 1$) an end correction of $8/(3\pi)d_0$, which would lead to an effective length of 7.56 mm. The observed reduction of the effective length with non-sharp edges has already been seen by other authors, see, e. g. [8]. In the analogy of the mass-spring-damper system discussed in Sec. 2, this means that less mass in the neck is taking in the oscillation with increasing the chamfer size.

Moreover, a reduction of the non-linear resistance can be observed in the presence of a chamfer. As discussed in Sec. 2, the non-linear resistance results from the flow separation the resonator edges. Two velocity field snapshots during the outflow for a sharp and a 1-mm-chamfered edge case with 119.7 dB excitation are presented in Fig. 4. In the sharp edge case visualized in Fig. 4(a), it can be observed that the flow separates at both the inner and the outer edge. Two large recirculation zones are temporally formed downstream of the respective edge. One of these zones is located in front of the resonator mouth and the other in the neck. Chamfering the sharp edges produces four obtuse edges that cause the flow to separate with smaller recirculation zones; see Fig. 4(b). The observed contraction of the stream motivates a comparison with the quasi-static theory including the vena contracta effect. The vena contracta for large amplitudes for sharp edges is about 0.70 while it is 0.95 for chamfered edges [17]. Since the non-linear losses scale approximately linear with the square of the jet velocity, the non-linear residence is inversely proportional to the square of the vena contracta factor. This explains the observed difference in the non-linear residence for high amplitudes by a factor of around two, see Fig. 3 and discussion below.

In the non-linear regime, increasing the amplitude always promotes the separation and, thus, leads to higher non-linear losses. This results in larger resistance values for higher excitation amplitudes in all cases, see Fig. 3. If the resonator is normally damped, the normalized acoustic resistance $\Re(Z)$ is below unity – the optimal resistance value for normal incident acoustic waves, i. e., $\Re(Z) < 1$. In that case, the increase of the acoustic resistance leads to a lower gain of the reflection coefficient, as it can be seen in the right columns of Figs. 2 and 3. This lower gain means that a higher proportion of the acoustic energy is dissipated. The situation changes in the over-damped case where $\Re(Z) > 1$ (c. f. left column in Figs. 2 and 3): Here, the additional non-linear resistance leads to a decrease in absorption. The normal and over-damped cases can also be distinguished by the examination the phase curve of the reflection coefficient $\angle R$. These phase angles differ from each other close to the eigenfrequency. In the over-damped case, it is 0 whereas it is $-\pi$ in the normal damped case. In both cases, the waves f and g are in phase – i. e., $\angle R = 0 \pmod{2\pi}$ – away from the eigenfrequency.

With the 1 mm-chamfer, none of the investigated SPLs lead to an over-damped behavior, whereas both non-linear cases are in the over-damped region for the sharp edge geometry. Notice that not only the non-linear but also the linear resistance varies with the edge profile. For instance, linear resistance decreases by 11% and 22% for the cases of 0.35 mm and 1.0 mm–chamfers, respectively. This shows that increasing the chamfer size reduces the thermo-viscous effect around the neck. Yet the impact on the resistance becomes more striking in the non-linear regime caused by a reduction of shedding. With the 0.35 mm-chamfer, the non-linear resistance is reduced by approximately 47% and 55% for the 115.3 dB and 119.7 dB case, respectively. A reduction of 57% and 70% is measured with the 1 mm-chamfer. The stated values correspond to experimental data. The magnitudes are similar for the simulation. Mainly, the presence of a chamfer reduces the non-linear losses significantly. The actual length of the chamfer also influences this reduction but in a minor manner. Moreover, it can be observed that the relative reduction is larger for higher SPL. This fits well to the above discussed flow properties: the strong separation with its large recirculation zones causes the high non-linear acoustic absorption in the sharp edge case. Much less energy is taken from the acoustics by the four separation areas with little recirculation in the chamfered case. The separation process itself is mainly determined by the sharpness of the edge.

5. Conclusion and Outlook

The influence of the edge shape of a Helmholtz resonator has been investigated by means of both experiments and LES simulations. To study this influence, various combinations of necks with different chamfer sizes and backing volumes have been considered. By variation of the SPL, the linear regime, where thermo-viscous losses are dominant, as well as the non-linear regime, where vortex shedding leads to additional losses, have been included.

In the linear regime, the results obtained from both methods match very well. The results agree qualitatively in the non-linear regime as well, even though the absolute values slightly disagree. The simulations overpredict the non-linear resistance. The reason for this disagreement is topic of ongoing research. Nevertheless, the following statements are supported equally by both the experimental and numerical investigations.

By increasing the chamfer size, a shift towards higher eigenfrequency frequencies has been observed. This shift occurs due to the fact that the oscillating mass in the neck is reduced, i. e., the effective length is shortened. This reduction is in good agreement with other correlation available in the literature.

Another important observation is that a chamfered edge profile reduces the vortex shedding in the resonator neck significantly. Depending on the SPL, the chamfered edge profile reduces the non-linear resistance about the half of its value compared to the sharp edge case. This reduction is mainly due to presence of the chamfer, but depends only weakly on its length. To the authors' knowledge, this is the first time that this effect has been quantified for the Helmholtz resonator.

Acknowledgments

Financial support has been provided by the German Research Foundation (Deutsche Forschungsgemeinschaft – DFG) in the framework of the Sonderforschungsbereich Transregio 40, Project A3. The presented work is part of the Marie Curie Initial Training Network Thermo-acoustic and aero-acoustic non-linearities in green combustors with orifice structures (TANGO). We gratefully acknowledge the financial support from the European Commission under call FP7-PEOPLE-ITN-2012. Furthermore, the authors would like to thank the Leibniz Supercomputing Centre (LRZ) for the access to its cluster system.

REFERENCES

1. Hersh, A. S., Walker, B. E. and Celano, J. W. Helmholtz Resonator Impedance Model, Part 1: non-linear Behavior. *AIAA Journal*, **41**(5), 795–808, (2003).
2. Tang, P. K. and Sirignano, W. A. Theory of a Generalized Helmholtz Resonator. *Journal of Sound and Vibration*, **26**(2), 247–262, (1972).
3. Helmholtz, H. L. F. *On the Sensations of the Tone As a Psychological Basis for the Theory of Music (Third Edition)*, Longmans, Green and Co., Chp. 3, (1895).
4. Rayleigh, J. W. S. *The Theory of Sound (Second Edition)*, Macmillan and Co., Chp. XVI, (1896).
5. Ingard, U. and Labate, S. Acoustic Circulation Effects and the non-linear Impedance of Orifices, *Journal of Acoustical Society of America*, **22**(2), 211–218, (1950).
6. Ingard, U. and Ising, H. Acoustic Nonlinearity of an Orifice, *Journal of Acoustical Society of America*, **42**(1), 6–17, (1967).
7. Disselhorst, J. H. M. and van Wijngaarden, L. Flow in the exit of open pipes during acoustic resonance, *Journal of Fluid Mechanics*, **99**, 293–319, (1980).
8. Keller, J. J. and Zauner, E. On the Use of Helmholtz Resonators as Sound Attenuators, *Zeitschrift für angewandte Mathematik und Physik ZAMP*, **46**(3), 297–327, (1995).
9. Garrison, G. D., Schnell, A. C., Baldwin, C. D. and Russell, P. R. Suppression of Combustion Oscillations with Mechanical Damping Devices, *Interim Report PWA FR-3299, Pratt & Whitney Aircraft*, (1969).
10. Peters, M. C. A. M., Hirschberg, A., Reijnen, A. J. and Wijnands, A. P. J. Damping and reflection coefficient measurements for an open pipe at low Mach and low Helmholtz numbers, *Journal of Fluid Mechanics*, **256**, 499–534, (1993).
11. Jang, S.-H. and Ih, J.-G. On the multiple microphone method for measuring in-duct acoustic properties in the presence of mean flow, *Journal of Acoustical Society of America*, **103**(3), 1520–1526, (1998).
12. Aurégan, Y. and Leroux, M. Failures in the discrete models for flow duct with perforations: An experimental investigation, *Journal of Sound and Vibration*, **265**, 109–121, (2003).
13. OpenFOAM (Open Field Operation and Manipulation), see <http://www.openfoam.org>.
14. Förner, K. and Polifke, W. Aero-Acoustic Characterization of Helmholtz Resonators in the Linear Regime with System Identification *Proceedings of the 22th International Congress on Sound and Vibration*, (2015).
15. Polifke, W., Wall, C. and Moin, P. Partially Reflecting and Non-Reflecting Boundary Conditions for Simulation of Compressible Viscous Flow, *Journal of Computational Physics*, **213**, 437–449, (2006).
16. Ingard, U. On the Theory and Design of Acoustic Resonators, *Journal of Acoustical Society of America*, **25**(6), 1037–1061, (1953).
17. Blevins, R. D. *Applied Fluid Dynamics Handbook*, Van Nostrand Reinhold, NY, (1984).